

Features of magnetic field switchbacks in relation to the local-field geometry of large-amplitude Alfvénic oscillations:
Wind and *PSP* observations

SOFIANE BOUROUAINE,¹ JEAN C. PEREZ,² NOUR E. RAOUFI,¹ BENJAMIN D. CHANDRAN,³ STUART D. BALE,⁴ AND
MARCO VELLI⁵

¹*Johns Hopkins Applied Physics Laboratory, 11100 Johns Hopkins Road, Laurel, MD, 20723, USA*

²*Department of Aerospace, Physics and Space Sciences, Florida Institute of Technology, 150 W University Blvd, Melbourne, FL, 32901, USA*

³*Department of Physics and Astronomy, University of New Hampshire, Durham, NH 03824, USA*

⁴*Space Sciences Laboratory, University of California, Berkeley, CA 94720, USA*

⁵*Earth, Planetary, and Space Sciences, University of California, Los Angeles Los Angeles, CA 90095, USA*

ABSTRACT

In this letter we report observations of magnetic switchback (SB) features near 1 au using data from the *Wind* spacecraft. These features appear to be strikingly similar to the ones observed by the Parker Solar Probe mission (PSP) closer to the Sun: namely, one-sided spikes (or enhancements) in the solar-wind bulk speed V that correlate/anti-correlate with the spikes seen in the radial-field component B_R . In the solar-wind streams that we analyzed, these specific SB features near 1 au are associated with large-amplitude Alfvénic oscillations that propagate outward from the sun along a local background (prevalent) magnetic field \mathbf{B}_0 that is nearly radial. We also show that, when \mathbf{B}_0 is nearly perpendicular to the radial direction, the large amplitude Alfvénic oscillations display variations in V that are two-sided (i.e., V alternately increases and decreases depending on the vector $\Delta\mathbf{B} = \mathbf{B} - \mathbf{B}_0$). As a consequence, SBs may not appear always as one-sided spikes in V , especially at larger heliocentric distances where the local background field statistically departs from the radial direction. We suggest that SBs can be well described by large-amplitude Alfvénic fluctuations if the field rotation is computed with respect to a well determined local background field that, in some cases, may deviate from the large-scale Parker field.

Keywords: TBA

1. INTRODUCTION

Near the Sun, at heliocentric distances below ~ 0.17 au, *Parker Solar Probe* (PSP, Fox et al. 2016) observes many intervals of slow wind where the bulk flow suddenly increases associated with temporary radial magnetic field reversals. These observed features were interpreted as magnetic switchbacks (SBs) (e.g., Bale et al. 2019; Kasper et al. 2019; Dudok de Wit et al. 2020). Also, these observed SBs are characterized by a high degree of Alfvénicity. The word “Alfvénicity” is commonly related to the characteristics of Alfvén waves (with finite or small amplitude), which are an exact solution to the Magneto-hydrodynamics (MHD) equations (Walén 1944; Goldstein et al. 1974; Barnes

& Hollweg 1974). These Alfvén waves are characterized by the following properties: 1) they satisfy Walén relations, $\Delta\mathbf{V} = \pm\Delta\mathbf{B}/\sqrt{\mu_0\rho}$, where $\Delta\mathbf{V}$ and $\Delta\mathbf{B}$ are velocity and magnetic field perturbations around the background, respectively, and μ_0 is vacuum’s magnetic permeability; 2) they have constant mass density, ρ , constant pressure, p , and constant magnetic field strength, $|\mathbf{B}|$; and 3) they propagate with a group velocity, called Alfvén velocity, $\mathbf{V}_A = \pm\mathbf{B}_0/\sqrt{\mu_0\rho}$, i.e., either parallel (for $\Delta\mathbf{V} = -\Delta\mathbf{B}\sqrt{\mu_0\rho}$) or anti-parallel (for $\Delta\mathbf{V} = +\Delta\mathbf{B}\sqrt{\mu_0\rho}$) to the local background magnetic field \mathbf{B}_0 . Several in-situ measurements have revealed the existence of Alfvén waves in the solar wind that propagate mainly outward from the Sun (see e.g., Bavassano et al. 1998), which means the perturbed fields $\Delta\mathbf{V}$ and $\Delta\mathbf{B}$ either anti-correlate (when $B_{0R} > 0$) or positively correlate (when $B_{0R} < 0$). Here B_{0R} is the component of \mathbf{B}_0 along the radial direction pointing outward from the Sun.

SBs have been previously observed over a wide range of heliocentric distances, (see, e.g., Borovsky 2016), near 0.3 au (Horbury et al. 2018), near 1 au (Kahler et al. 1996; Gosling et al. 2009) and beyond 1 au (Balogh et al. 1999; Yamauchi et al. 2004; Neugebauer & Goldstein 2013). In *PSP* observations, the electron strahl pitch angle distributions was found to follow the magnetic field through SBs (Whittlesey et al. 2020). Also, within SBs, Alfvénic fluctuations at inertial-range scales appear to have correlations corresponding to fluctuations propagating towards the Sun (Bourouaine et al. 2020; McManus et al. 2020).

Several scenarios have been proposed to explain the origin of SBs. Some studies suggest that SBs are caused by magnetic reconnection as a result of interchange between open and closed magnetic field structures at the base of the solar corona, which are then convected outward with the solar wind (e.g., Fisk & Kasper 2020; Zank et al. 2020; Drake et al. 2021; Liang et al. 2021). Other scenarios propose that SBs are created locally in the solar wind as a result, for example, of the radial evolution of Alfvénic turbulence in the expanding solar wind (Landi et al. 2005, 2006; Squire et al. 2020; Shoda et al. 2021; Mallet et al. 2021) or due to shear-driven dynamics (see e.g., Landi et al. 2006; Ruffolo et al. 2020; Schwadron & McComas 2021).

Unlike some previous works in which SBs are attributed to field deflections with respect to the large-scale Parker field (see e.g., Balogh et al. 1999; Borovsky 2016; Matteini et al. 2014), in this letter we analyze the field rotation with respect to a local background field, that may deviate from the large-scale Parker spiral due to the presence of large-scale fluctuations (e.g., waves having periods of a few days Coleman (1968).)

In this letter we use *Wind* data to show that some of the SB features observed recently by *PSP* near the Sun, such as the one-sided spikes (or enhancements) in the bulk flow that correlate/anti-correlate with the spikes seen in the radial component of the magnetic field, are also observed near 1 au (where the large-scale Parker field is not nearly radial). Here, we demonstrate that such SBs features seem to show up naturally when large-amplitude Alfvénic oscillations propagate anti-sunward along a nearly radial (or anti-radial) local prevalent field. Those SB features are also compared with the ones observed by *PSP* during its first perihelion. In the following section, we present the analysis method and our findings. Then, in section 3, we summarize and discuss the obtained results.

2. DATA ANALYSIS AND RESULTS

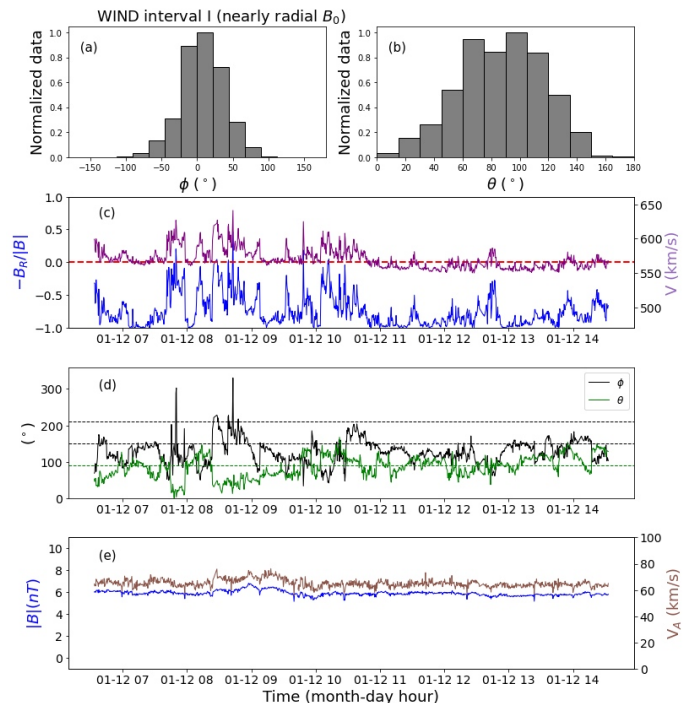


Figure 1. Eight-hours long time-interval I of *Wind* observations: Panels from top to bottom correspond to (a) and (b) Histograms of the ϕ and θ angle, (c) the normalized radial component of the magnetic field $-B_R/|\mathbf{B}|$ (blue line) and the bulk flow V (purple line), (d) The azimuth angle ϕ (black) and the polar angle θ (green), respectively, and (e) the magnitude of the magnetic field vector $|\mathbf{B}|$ (Blue) and the Alfvén speed V_A (Brown).

We use plasma and field measurements from *Wind* to investigate the presence of SB features near 1 au. We use the combined data of magnetic field vector and the plasma parameters provided with time resolution of about 24.7 sec (Lepping et al. 1995). Here the vector fields are given in the Geocentric Solar Ecliptic system (GSE), i.e., the x -axis pointing from the Earth toward the Sun, the y -axis is chosen to be in the ecliptic plane pointing towards dusk (opposing planetary motion), and the z -axis is parallel to the ecliptic north. For the sake of comparison with SBs observed by *PSP*, we will also use plasma and magnetic field data from *PSP* during its first encounter (Case et al. 2020; Bale et al. 2016). The *PSP* data shown here are provided in the radial-tangential-normal (RTN) coordinate system. Here, we lower the resolution of *PSP* data to the plasma resolution of *Wind*, namely, 24.7 s for a better comparison.

Figure 1 displays results from an eight-hours long time-interval on January 12 in 2002 of *Wind* measurements. Panels (a) and (b) show the histograms of the azimuth angle ϕ and the polar angle θ , respectively. The azimuth angle ϕ is defined as the angle between the ra-

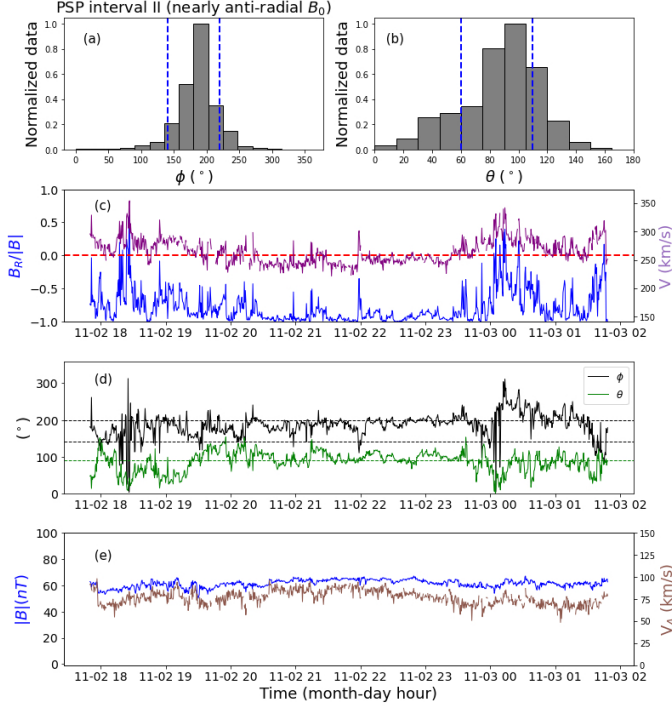


Figure 2. Eight-hours long time-interval II of *PSP* observations: Panels from top to bottom correspond to (a) and (b) Histograms of the ϕ and θ angle, (c) the normalized radial component of the magnetic field $B_R/|\mathbf{B}|$ (blue line) and the bulk flow V (purple line), (d) The azimuth angle ϕ (black) and the polar angle θ (green), respectively, and (e) the magnitude of the magnetic field vector $|\mathbf{B}|$ (Blue) and the Alfvén speed V_A (Brown).

dial direction outward from the Sun ($-x$ direction) and the projected component of \mathbf{B} onto the $x-y$ plane, and the polar angle θ is the angle between polar axis, z , and the instantaneous vector field \mathbf{B} . From the histogram plots, the most prevalent values of both angles correspond to $\phi \simeq 5^\circ$ and $\theta \simeq 86^\circ$. Here, the local mean field \mathbf{B}_0 (averaged over the eight-hours long time-interval) field is nearly radial (nearly parallel to the bulk velocity), and lies nearly on the ecliptic plane.

Panel (c) of Figure 1 displays the normalized x-component of the field $B_x/|\mathbf{B}| = -B_R/|\mathbf{B}|$ (where B_R is the radial component) versus time. The normalized x-component $B_x = -B_R$ oscillates in a one-sided fashion, showing the kind of spikes that at some points can even exceed zero value and flip the sign. In the same figure we plot the flow speed V (purple line) that also oscillates in one side fashion following the spikes in $-B_R/|\mathbf{B}|$. Panel (d) of Figure 1 shows that the spikes in B_x are mostly associated with the deviations of the angles ϕ and θ from their prevalent values.

As shown in panel (e) of Figure 1 these field oscillations occur at nearly constant B^2 and constant

Alfvén speed, $V_A = B/\sqrt{\mu_0\rho}$, where ρ is the mass density of protons. These are highly Alfvénic oscillations with a normalized cross helicity of $\sigma_c = -0.9$, where $\sigma_c = 2\langle(\delta\mathbf{V} \cdot \delta\hat{\mathbf{B}})/(\delta V^2 + \delta\hat{\mathbf{B}}^2)\rangle$, and $\delta\mathbf{V} = \mathbf{V} - \mathbf{V}_0$ ($\delta\hat{\mathbf{B}} = (\mathbf{B} - \mathbf{B}_0)/\sqrt{\mu_0\rho_0}$) is the fluctuating velocity field (magnetic field, converted to velocity unit). Here, \mathbf{V}_0 and ρ_0 are the mean quantities (averaged over the eight hours long time-interval) of the velocity and mass density, respectively. The Alfvénic structures measured in this interval propagate outward from the Sun (as $\sigma_c < 0$ and $-B_{0x} = B_{0R} > 0$).

The features shown in Figure 1 appear to be similar to the ones observed by *PSP* near the Sun at ~ 0.17 au (see, e.g., Bale et al. 2019; Kasper et al. 2019). For the sake of comparison, in Figure 2, we plot the same parameters as those shown in Figure 1 but from an eight-hour long time interval of *PSP* during its first encounter on November 2 and 3 in 2018. Analysis of this interval shows that the local background field is nearly anti-radial corresponding to prevalent azimuth angle $\phi = 175^\circ$ (and $\theta = 88^\circ$). Here the ϕ angle is defined with respect to the radial axis of an RTN coordinate system, with $B_R \equiv -B_x$. The oscillations of the radial component B_R correlate with the one sided enhancement in the bulk flow. These oscillations are also highly Alfvénic (with $\sigma_c = 0.9$) and propagate outward from the Sun (as $\sigma_c > 0$ and $B_{0R} < 0$).

In order to check how the geometry of the local background magnetic field may affect the overall features that are often associated with SBs near the Sun, we select another eight-hour long time interval observed by *Wind* (shown in Figure 3) in which the oscillations are also highly Alfvénic (with $\sigma_c = -0.9$) and the local mean field is nearly perpendicular to the radial direction (and the solar wind bulk velocity). From the top panels of Figure 3 we see that the most frequent value of ϕ (θ) is $\sim 100^\circ$ ($\sim 93^\circ$) corresponding to local background field \mathbf{B}_0 that is nearly perpendicular to the radial direction. In this case, the Alfvénic oscillations propagate anti-parallel to \mathbf{B}_0 .

For this geometrical configuration of the local field \mathbf{B}_0 , the bulk flow and the radial component of the field do not show one-sided spikes as seen from Figures 1 and 2.

In the following we propose a picture, illustrated in Figure 4, to explain how the local background field direction and the corresponding anti-sunward Alfvénic oscillations (in the case when \mathbf{B}_0 is nearly radial or anti-radial) may provide the above patterns of the bulk flow and the radial component of the field. For the sake of simplicity, we assume that the local background field \mathbf{B}_0 and the oscillating field vector \mathbf{B} both lie nearly in the ecliptic plane. The demonstration below can still hold

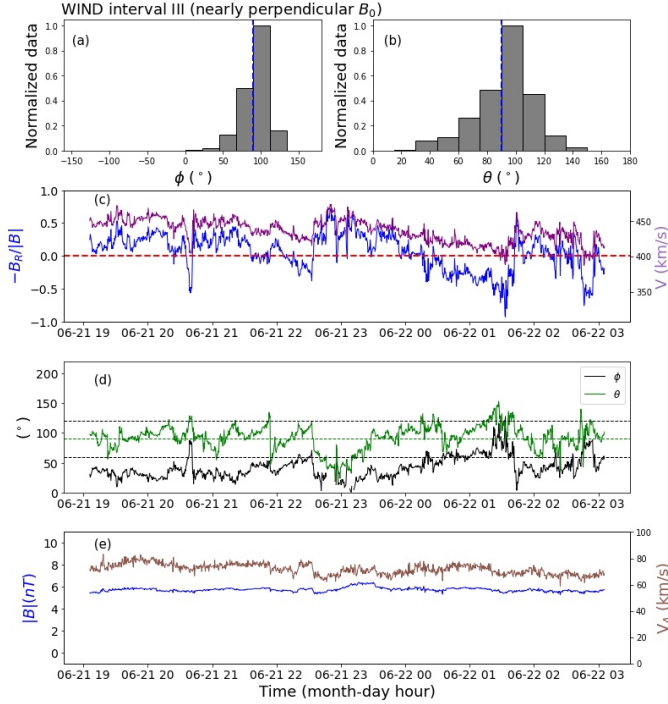


Figure 3. Interval III of *Wind* observations: Panels from top to bottom correspond to (a) and (b) Histograms of the ϕ and θ angle, (c) the normalized radial component of the magnetic field $-B_R/|\mathbf{B}|$ (blue line) and the bulk flow V (purple line), (d) The azimuth angle ϕ (black) and the polar angle θ (green), respectively, and (e) the magnitude of the magnetic field vector $|\mathbf{B}|$ (Blue) and the Alfvén speed V_A (Brown).

even when the oscillating field \mathbf{B} is out of the ecliptic (i.e., with polar angle $\theta \neq 90$).

Figure 4a shows the case when the instantaneous magnetic field \mathbf{B} (shown in black) oscillates in the shaded area around a nearly radial prevalent (background) magnetic field \mathbf{B}_0 (shown in red) (nearly parallel to the mean bulk flow velocity, \mathbf{V}_0 , shown in green). If we assume that these oscillations are purely Alfvénic and propagate outward from the Sun, then the fluctuating magnetic field vector $\Delta\hat{\mathbf{B}} = (\mathbf{B} - \mathbf{B}_0)/\sqrt{\mu_0\rho}$ and the fluctuating bulk velocity vector $\Delta\mathbf{V} = \mathbf{V} - \mathbf{V}_0$ have an opposite sign, i.e., $\Delta\mathbf{V} = -\Delta\mathbf{B}$ (in the unit where $\sqrt{\mu_0\rho} = 1$). Here \mathbf{V} is the instantaneous measured bulk flow vector. In this case, because the magnetic field is nearly radial, the instantaneous field \mathbf{B} oscillates around \mathbf{B}_0 within the shaded area, producing the vector changes $\Delta\mathbf{B}_1$ (counter-clockwise) and $\Delta\mathbf{B}_2$ (clockwise). In such rotations of \mathbf{B} the radial component $B_R/|\mathbf{B}|$ (here $|\mathbf{B}|$ is constant) varies between positive and negative values for some large rotations near or larger than 90° leading to the kind of one-sided oscillations in B_R that we see in the second panels of Figures 1 and 2. Interestingly, in this \mathbf{B}_0 configuration, it seems that the fluctuating

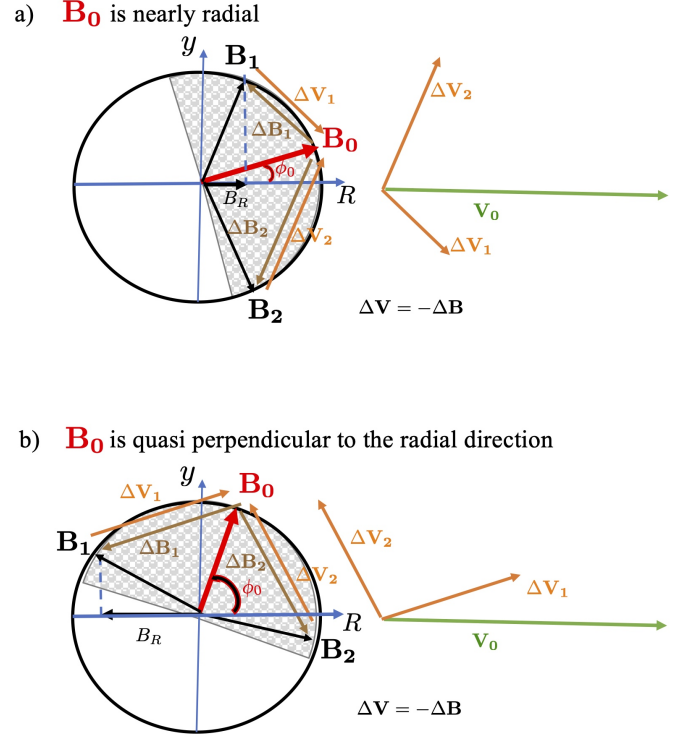


Figure 4. Sketch describes how the radial field component $B_x/|B|$ and the fluctuating bulk velocity $\Delta\mathbf{V}_1 = -\Delta\mathbf{B}_1$ and $\Delta\mathbf{V}_2 = -\Delta\mathbf{B}_2$ (orange vectors) add to the local mean bulk velocity \mathbf{V}_0 (Green vector) during the oscillation of the instantaneous magnetic field vector \mathbf{B}_1 and \mathbf{B}_2 (black vectors) around the local background magnetic field vector \mathbf{B}_0 for the case (a) where \mathbf{B}_0 is nearly radial, and for case (b) where \mathbf{B}_0 is nearly perpendicular to the radial direction (of the bulk flow direction). Here $\Delta\mathbf{B}_1$ and $\Delta\mathbf{B}_2$ are normalized to velocity unit.

velocity vectors $\Delta\mathbf{V}_1 = -\Delta\mathbf{B}_1$ and $\Delta\mathbf{V}_2 = -\Delta\mathbf{B}_2$ (orange vectors) both contribute to the enhancement of the bulk flow \mathbf{V}_0 , leading to one-sided increases of the bulk flow that correlates with the spikes of $-B_R$. Note that this explanation holds even when \mathbf{B}_0 is nearly anti-radial and $\sigma_c > 0$ for anti-sunward propagating Alfvénic oscillations, except that the one-sided increases of the bulk flow correlates with the spikes of B_R .

However, when the local background field \mathbf{B}_0 is nearly perpendicular to the radial direction (or to the bulk velocity) then the oscillating instantaneous field \mathbf{B} around \mathbf{B}_0 can cover a wide range in which the radial component B_R oscillates between positive and negative values in more or less equivalent ways. In such case, the B_R component will not show a one sided pattern as shown in the second panel of Figure 3. Moreover, the counter-clockwise (clockwise) rotation of the field \mathbf{B} with respect to \mathbf{B}_0 produces a change in the velocity $\Delta\mathbf{V}_1$ ($\Delta\mathbf{V}_2$) that leads to either increase (decrease) in the bulk velocity

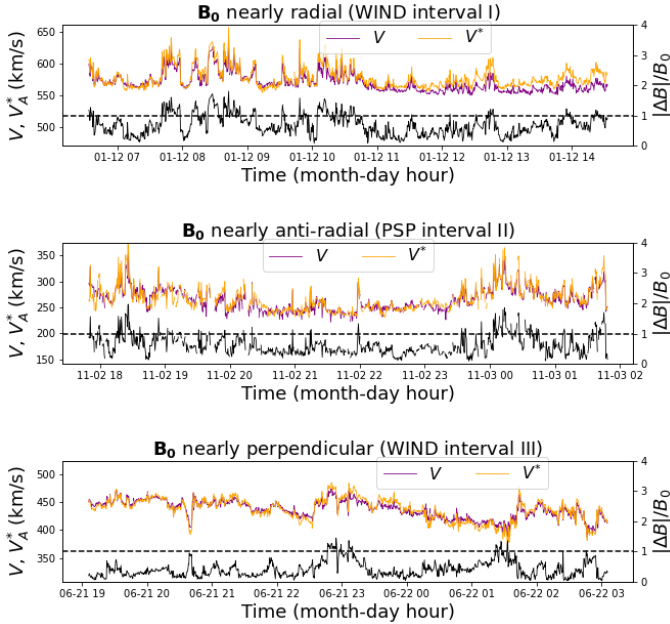


Figure 5. Panels from top to bottom correspond to the measured bulk flow V (purple line) and the reconstructed bulk flow V^* from changes in magnetic field ΔB for interval I, II and III. The horizontal dash line represent the mean bulk flow V_0 considered for the reconstruction of V^* .

when $\sigma_c < 0$ (or either decrease (increase) in the bulk velocity when $\sigma_c > 0$) for such a \mathbf{B}_0 geometry.

To further verify the picture given above we estimate the fluctuating bulk velocity, $\Delta \mathbf{V}^*$, from the empirical fluctuating magnetic field $\Delta \mathbf{B}$ as $\Delta \mathbf{V}^* = \alpha \Delta \mathbf{B}$ (in the unit $\sqrt{\mu_0 \rho} = 1$), where $\alpha = -1$ ($\alpha = 1$) when \mathbf{B}_0 is near radial (anti-radial). This approximate estimation is based on the assumption that the oscillations are entirely Alfvénic and with anti-sunward propagation at least for the case when \mathbf{B}_0 is nearly radial or anti-radial. Therefore, we estimate the modeled bulk flow, V^* , as $V^* = |\mathbf{V}_0 + \Delta \mathbf{V}^*|$ for the three intervals we used above. Here \mathbf{V}_0 is the mean bulk flow velocity. Figure 5 displays the velocity V^* , obtained from the model (orange line), and the bulk flow V (purple line) obtained from direct measurements for the three intervals I (*Wind*), II (*PSP*) and III (*Wind*) used in Figures 1, 2 and 3, respectively. Figure 5 shows that the modeled velocity, V^* and the empirical bulk flow V nearly overlap. It is clear that the enhanced bulk flow in most part of the signal in the two top panels can be well explained by the propagation of Alfvén waves along a nearly radial local background field \mathbf{B}_0 for the *Wind* and the *PSP* measurements. In addition, in the bottom panel of Figure 5 we plot the ratio $\frac{|\Delta B|}{B_0} = 2 \sin(\eta/2)$, where η is the rotational angle, i.e., the angle between the instantaneous field vector \mathbf{B} and the local prevalent field \mathbf{B}_0 .

The figure clearly shows that the significant enhancement in the bulk flow occurs when $\Delta B/B_0 \gtrsim 1$ (one side spikes) when \mathbf{B}_0 is nearly radial (or anti-radial) (as shown for interval I and II). However, the bulk flow may significantly increase or decrease when $\Delta B/B_0 \gtrsim 1$ and \mathbf{B}_0 is nearly perpendicular.

3. SUMMARY AND DISCUSSION

In this work we report observations of SB features near 1 au that are very similar to those observed by *PSP* near the Sun. We have shown that a property often linked to the presence of SBs near the Sun, which is the one-sided spikes (or enhancements) in the bulk flow V that correlate/anti-correlate with the spikes seen in the radial field component B_R , can be caused by the presence of large-amplitude Alfvénic oscillations (with $|\Delta \mathbf{B}|/|\mathbf{B}_0| \sim 1$) propagating outward from the Sun along a local background field \mathbf{B}_0 that is nearly radial (or anti-radial). This property does not show up if the local prevalent field \mathbf{B}_0 is not sufficiently radial.

Matteini et al. (2014) studied the dependence of solar wind speed on the magnetic field orientation in Alfvénic solar wind streams at high latitudes. The authors proposed that the enhancement in the bulk flow depends on the position of the instantaneous field \mathbf{B} with respect to a local mean field that is not assumed to be radial (but nearly follows Parker field direction at 1 au). In our analysis we rather focused on the geometry of the local background field, \mathbf{B}_0 , of Alfvénic oscillations, and showed how that geometry affects the profile of the solar wind bulk flow when the field rotates strongly with respect to \mathbf{B}_0 .

From our analysis, we conjecture that SBs (or at least a subset of SBs) can be sudden large rotations of the field (with $|\Delta \mathbf{B}|/B_0 \sim 1$) associated with large-amplitude Alfvénic oscillations that propagate outward from the Sun along a well determined local background field, but this local field may in some cases deviate from the Parker spiral due to the presence of larger-scale solar wind oscillations, e.g., oscillations with periods of days (Coleman 1968; Bruno & Carbone 2005). Also, the one-sided spikes in the bulk flow speed that often appear to correlate/anti-correlate with the radial magnetic field component cannot be used as the main criterion for the determination of SB field reversals.

SBs (or at least a subset of them) are strongly connected to large-amplitude Alfvénic oscillations, which therefore makes understanding the evolution of the large-amplitude Alfvénic fluctuations in the solar wind a necessary part of understanding the dynamics and evolution of SBs. For example, recent studies proposed that these type of oscillations can be generated due

to the solar wind expansion (e.g., [Squire et al. 2020](#); [Mallet et al. 2021](#)).

The authors would like to thank Dr. C. H. k. Chen for his valuable discussion. SB was supported by NASA

grants 80NSSCK0012 and Parker Solar Probe as part of of NASA’s Living with a Star (LWS) program (contract NNN06AA01C). JCP was partially supported by NASA grant 80NSSCK0012 and NSF grant AGS-1752827. BC was supported in part by NASA grants NNN06AA01C and 80NSSC19K0829.

REFERENCES

- Bale, S. D., Goetz, K., Harvey, P. R., et al. 2016, *Space Sci Rev*, 204, 49
- Bale, S. D., Badman, S. T., Bonnell, J. W., et al. 2019, *Nature*, 576, 237
- Balogh, A., Forsyth, R. J., Lucek, E. A., Horbury, T. S., & Smith, E. J. 1999, *Geophys. Res. Lett.*, 26, 631
- Barnes, A., & Hollweg, J. V. 1974, *J. Geophys. Res.*, 79, 2302
- Bavassano, B., Pietropaolo, E., & Bruno, R. 1998, *J. Geophys. Res.*, 103, 6521
- Borovsky, J. E. 2016, *Journal of Geophysical Research (Space Physics)*, 121, 5055
- Bourouaine, S., Perez, J. C., Klein, K. G., et al. 2020, *ApJL*, 904, L30
- Bruno, R., & Carbone, V. 2005, *Living Reviews in Solar Physics*, 2, 4
- Case, A. W., Kasper, J. C., Stevens, M. L., et al. 2020, *ApJS*, 246, 43
- Coleman, Paul J., J. 1968, *ApJ*, 153, 371
- Drake, J. F., Agapitov, O., Swisdak, M., et al. 2021, *A&A*, 650, A2
- Dudok de Wit, T., Krasnoselskikh, V. V., Bale, S. D., et al. 2020, *ApJS*, 246, 39
- Fisk, L. A., & Kasper, J. C. 2020, *ApJL*, 894, L4
- Fox, N. J., Velli, M. C., Bale, S. D., et al. 2016, *SSRv*, 204, 7
- Goldstein, M. L., Klimas, A. J., & Barish, F. D. 1974, in *Solar Wind Three*, ed. C. T. Russell, 385–387
- Gosling, J. T., McComas, D. J., Roberts, D. A., & Skoug, R. M. 2009, *ApJL*, 695, L213
- Horbury, T. S., Matteini, L., & Stansby, D. 2018, *MNRAS*, 478, 1980
- Kahler, S. W., Crooker, N. U., & Gosling, J. T. 1996, *J. Geophys. Res.*, 101, 24373
- Kasper, J. C., Bale, S. D., Belcher, J. W., et al. 2019, *Nature*, 576, 228
- Landi, S., Hellinger, P., & Velli, M. 2005, in *ESA Special Publication*, Vol. 592, *Solar Wind 11/SOHO 16, Connecting Sun and Heliosphere*, ed. B. Fleck, T. H. Zurbuchen, & H. Lacoste, 785
- Landi, S., Hellinger, P., & Velli, M. 2006, *Geophys. Res. Lett.*, 33, L14101
- Lepping, R. P., Acuña, M. H., Burlaga, L. F., et al. 1995, *Space Science Reviews*, 71, 207
- Liang, H., Zank, G. P., Nakanotani, M., & Zhao, L. L. 2021, *ApJ*, 917, 110
- Mallet, A., Squire, J., Chandran, B. D. G., Bowen, T., & Bale, S. D. 2021, *ApJ*, 918, 62
- Matteini, L., Horbury, T. S., Neugebauer, M., & Goldstein, B. E. 2014, *Geophys. Res. Lett.*, 41, 259
- McManus, M. D., Bowen, T. A., Mallet, A., et al. 2020, *ApJS*, 246, 67
- Neugebauer, M., & Goldstein, B. E. 2013, in *American Institute of Physics Conference Series*, Vol. 1539, *Solar Wind 13*, ed. G. P. Zank, J. Borovsky, R. Bruno, J. Cirtain, S. Cranmer, H. Elliott, J. Giacalone, W. Gonzalez, G. Li, E. Marsch, E. Moebius, N. Pogorelov, J. Spann, & O. Verkhoglyadova, 46–49
- Ruffolo, D., Matthaeus, W. H., Chhiber, R., et al. 2020, *ApJ*, 902, 94
- Schwadron, N. A., & McComas, D. J. 2021, *ApJ*, 909, 95
- Shoda, M., Chandran, B. D. G., & Cranmer, S. R. 2021, *ApJ*, 915, 52
- Squire, J., Chandran, B. D. G., & Meyrand, R. 2020, *ApJL*, 891, L2
- Walén, C. 1944, *Arkiv for Matematik, Astronomi och Fysik*, 30A, 1
- Whittlesey, P. L., Larson, D. E., Kasper, J. C., et al. 2020, *ApJS*, 246, 74
- Yamauchi, Y., Suess, S. T., Steinberg, J. T., & Sakurai, T. 2004, *Journal of Geophysical Research (Space Physics)*, 109, A03104
- Zank, G. P., Nakanotani, M., Zhao, L. L., Adhikari, L., & Kasper, J. 2020, *ApJ*, 903, 1